aerospace

MDPI

Article

Microstructural Evolution and Mechanical Properties of Ti_2AlNb/GH99 Superalloy Brazed Joints Using TiZrCuNi Amorphous Filler Alloy

Junjie Cai [1,2], Shengpeng Hu [2,3,4,*], Hongbing Liu [1,*], Danyang Lin [2,3], Wei Fu [2,3] and Xiaoguo Song [2,3,4]

[1] School of Materials Engineering, Shanghai University of Engineering Science, Shanghai 201620, China
[2] Shandong Provincial Key Lab of Special Welding Technology, Harbin Institute of Technology at Weihai, Weihai 264209, China
[3] State Key Laboratory of Advanced Welding and Joining, Harbin Institute of Technology, Harbin 150001, China
[4] Shandong Institute of Shipbuilding Technology, Weihai 264200, China
* Correspondence: sp_hu@hit.edu.cn (S.H.); lhongbing@163.com (H.L.)

Abstract: Dissimilar materials brazing of Ti_2AlNb alloy to GH99 superalloy is of great pragmatic importance in the aerospace field, especially the lightweight space aircraft components manufacturing. In this work, TiZrCuNi amorphous filler alloy was used as brazing filler, and experiments were carried out at different brazing temperatures and times to investigate the changes in interfacial structures and properties of the joints. The typical interfacial microstructure was Ti_2AlNb alloy/B2/β/Ti_2Ni (Al, Nb) + B2/β + (Ti, Zr)$_2$(Ni, Cu) + (Ti, Zr)(Ni, Cu)/(Cr, Ni, Ti) solid solution + (Ni, Cr) solid solution/GH99 superalloy when being brazed at 1000 °C for 8 min. The interfacial microstructure of the joints was influenced by diffusion and reaction between the filler alloy and the parent metal. The prolongation of brazing process parameters accelerated the diffusion and reaction of the liquid brazing alloy into both parent metals, which eventually led to the aggregation of (Ti, Zr)$_2$(Ni, Cu) brittle phase and increased thickness of Ti_2Ni (Al, Nb) layer. According to fracture analyses, cracks began in the Ti_2Ni (Al, Nb) phase and spread with it as well as the (Ti, Zr)$_2$(Ni, Cu) phase. The joints that were brazed at 1000 °C for 8 min had a maximum shear strength of ~216.2 MPa. Furthermore, increasing the brazing temperature or extending the holding time decreased the shear strength due to the coarse Ti_2Ni (Al, Nb) phase and the continuous (Ti, Zr)$_2$(Ni, Cu) phase.

Keywords: intermetallics; dissimilar alloys brazing; interfacial microstructure; fracture

check for updates

Citation: Cai, J.; Hu, S.; Liu, H.; Lin, D.; Fu, W.; Song, X. Microstructural Evolution and Mechanical Properties of Ti_2AlNb/GH99 Superalloy Brazed Joints Using TiZrCuNi Amorphous Filler Alloy. *Aerospace* **2023**, *10*, 73. https://doi.org/10.3390/aerospace10010073

Academic Editor: Khamis Essa

Received: 24 September 2022
Revised: 19 December 2022
Accepted: 4 January 2023
Published: 10 January 2023

1. Introduction

As demands for aerospace and nuclear energy industries have increased, more strict comprehensive performance of materials and structures is required. For example, technological advances such as advanced high thrust-to-weight ratio aero-engines strongly depend on new materials and structures with excellent overall performance such as low density, high strength, high-temperature resistance, and oxidation resistance [1].

A superalloy is a kind of high-temperature resistant metal material composed of Ni, Co, and other elements. Due to its good oxidation resistance, corrosion resistance, and excellent strength at high temperatures, it is often used in equipment such as aero-engine and industrial gas turbines [2]. GH99, a typical aging strengthening nickel-base superalloy, is mainly used in high-temperature structural materials such as aerospace turbines and power station turbines. However, the high density of GH99 superalloy alloy increased the part's weight and reduced the work's efficiency [3]. On the other hand, TiAl alloys have low room-temperature plasticity, fracture toughness, and poor high-temperature oxidation resistance, limiting their practical application [4]. To improve the properties of TiAl alloys, Nb and Zr have been added to enhance their room-temperature plasticity and high-temperature oxidation resistance [5]. Among the TiAl-based alloys, Ti_2AlNb alloy has attracted attention for its high-temperature strength, good anti-oxidation properties, and low density, with long-term service temperatures of up to 923 K–973 K [6]. Currently, Ti_2AlNb alloy has become the most promising lightweight material for aerospace applications [7]. Therefore, for the sake of weight reduction for some components, joining GH99 alloy to Ti_2AlNb alloy became one of the effective methods to achieve lightweight.

The joining of dissimilar alloys mainly includes diffusion bonding [8], arc welding [9], laser welding [10], friction welding [11], and brazing. As one of the cost-effective joining techniques, the brazing method [12,13] is often used to join Ni-based superalloys and TiAl-based alloys. Currently, the primary brazing alloys used for joining Ti-based or Ni-based superalloys are Ag-based, Au-based, Ni-based, and Ti-based alloys. Sequeiros et al. [14] used AgCuInTi filler alloy to join TiAl and Inconel 718 alloys. The hardness test showed that the joints microhardness rapidly reduced from the diffusion zone to the center of the brazing seam. The brittle phase in the joints was mainly the $AlNi_2Ti$ phase. Ren et al. [15] used AuNi filler alloy to join Ti_3Al and GH536 superalloys. The brazing seam was mainly composed of $AlNi_2Ti$ phase and Ni-Ti compounds. Liu et al. [16] used graphene-reinforced BNi-2 filler to join GH99 alloy. They found that the introduction of graphene reduced the precipitation of borides in the brazing seam, thereby increasing the joint strength. Li et al. [17] used amorphous filler alloy TiZrCuNiCo to connect TiAl intermetallic compounds. The joint produced a significant amount of Ti_2Cu/Ti_2Ni phase. They found that cracks initiated and propagated at the Ti_2Cu/Ti_2Ni phase. It was well known that Ag-based filler alloys had a lower service temperature, Au-based filler alloys were more expensive and Ni-based filler alloys had a high melting point. So, Ti-based filler alloys were chosen to join Ti-based alloys and Ni-based superalloys in this work. Nevertheless, there were few reports of studies on the brazing of TiAl intermetallic compounds with Ni-based alloys.

In this study, TiZrCuNi amorphous filler metal was selected to brazed Ti_2AlNb and GH99 superalloy. The microstructure evolution of joints during brazing was discussed. On the evolution of the interfacial microstructure and the mechanical characteristics of joints, the effects of the brazing parameters (temperature and time) were investigated.

2. Experiment

The materials used in this experiment were Ti_2AlNb alloy, GH99 superalloy, and commercially obtained TiZrCuNi filler alloy. The chemistry of the parent metals is listed in Table 1. In this work, Ti38.65Zr15.7Cu10.1Ni (wt.%) amorphous filler alloy was used to join Ti_2AlNb alloy and GH99 superalloy. Figure 1a shows the X-ray diffraction pattern taken from Ti35.5Zr38.65Cu15.70Ni10.10 (wt.%) alloy foil, which indicated the amorphous structure of the filler. The DSC result indicated that the brazing filler metal started to melt at 845 °C and turned to liquid at 853 °C, as shown in Figure 1b. In this experiment, the brazing temperature was chosen to be above 853 °C in order to allow the filler alloy to melt, based on the DSC test results.

Table 1. Chemical composition of the parent metals and filler alloy.

	Ti	Zr	Ni	Cu	Al	Nb	Cr	W	Co	Mo
Ti_2AlNb (at.%)	Bal.	—	—	—	11.72	32.31	—	—	—	1.7
GH99 (at.%)	1.42	—	Bal.	—	1.05	—	18.32	8.23	6.56	2.93

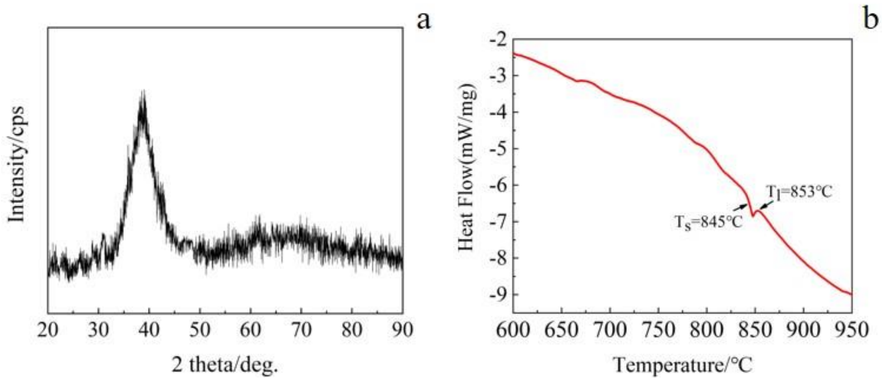

Figure 1. (**a**) XRD pattern and (**b**) DSC curve of Ti35.5Zr38.65Cu15.70Ni10.10 (wt.%) amorphous filler alloy.

GH99 superalloy and Ti_2AlNb alloy were cut into specimens with sizes of $15 \times 10 \times 5$ mm^3 and $5 \times 5 \times 5$ mm^3, respectively. The thickness of the amorphous TiZrCuNi filler alloy was 60 µm. Prior to brazing, Ti_2AlNb and GH99 superalloys were ground on sandpaper and subsequently polished. The polished parent metal and filler alloy were ultrasonically cleaned for 15 min in acetone and then dried with a hair dryer. Subsequently, the TiZrCuNi foil was sandwiched between GH99 superalloy and Ti_2AlNb alloy. The sample assembly is shown in Figure 2a. The vacuum level in the vacuum furnace, where the brazing experiments were conducted, was kept at (1.0–2.0) 10^{-3} Pa. Five brazing temperatures of 960, 980, 1000, 1020, and 1040 °C were chosen for the brazing experiments, along with five holding times of 4, 6, 8, 10, and 12 min. At the initiation of brazing, the furnace's heating was carried out at 10 °C/min to 800 °C and held for 10 min, and then the heating was continued at this rate to brazing temperature; hold at brazing temperature for the corresponding time, then cool down from brazing temperature to 200 °C with 5 °C/min, and finally cool down with the furnace to room temperature.

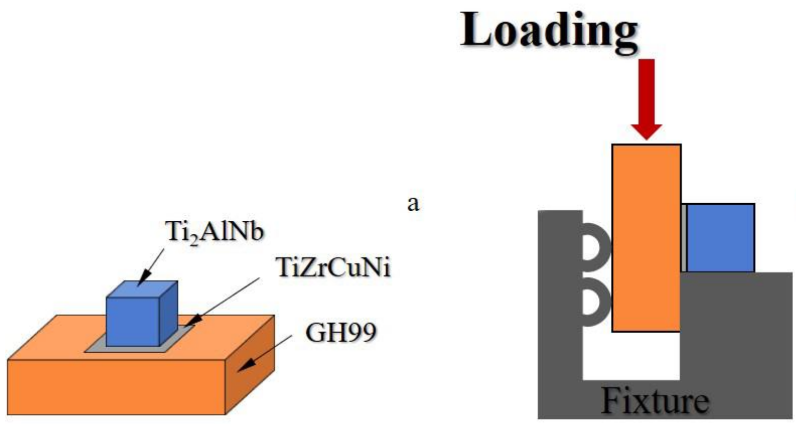

Figure 2. (**a**) Brazed joint assembly diagram; (**b**) shear test diagram.

The Ti_2AlNb/GH99 brazed joints were cut using a cutting machine and the interfacial microstructure was characterized by scanning electron microscopy (SEM, ZEISS, MERLIN Compact). An energy spectrometer (EDAX, OCTANE PLUS) was used to determine the phase composition of the brazed joints. The fracture was characterized by X-ray diffraction (XRD, DX-2700) to determine the interfacial phase's composition further. The shear test of brazed joints was conducted using a universal testing apparatus (Instron 5967) at room temperature with a constant shear speed of 0.5 mm/min. The assembly of the shear test specimen is illustrated in Figure 2b. Each group of experimental data of the shearing experiment was tested with at least five samples, and the average value was finally obtained as the final practical result. Shear test followed by characterization of the fracture using SEM to study the failure mode and fracture morphology of the joint.

3. Results and Discussion

3.1. Typical Interfacial Microstructure of Ti_2AlNb/TiZrCuNi/GH99 Joint

The Ti_2AlNb alloy and GH99 superalloy were successfully brazed using amorphous TiZrCuNi as the filler alloy, as illustrated in Figure 3a. The brazing seam could distinguish three zones in brazed joints according to the contrast of interfacial microstructure, which were named zone I (diffusion zone at Ti_2AlNb alloy side), zone II (reaction zone), and zone III (diffusion zone at GH99 side). From Figure 3b,d, it can be seen that Ti and Nb elements were mainly distributed in zone I, and their content gradually decreased in zone II and zone III. The Ti, Zr, Ni, Cu, Nb, and Al elements were mainly centered in the brazing seam. The distributions of the elements in the brazed joint indicated sufficient diffusion between the parent metal and the filler alloy. Combining Figure 3a,b,g, it was apparent that the black phase in zone II mostly contained Ti, Ni, and less Al, Nb. Despite the low levels of Cr and Co in the braze seam (zone II), the fact that Co was present in higher concentrations than Cr suggested that Co was more likely to diffuse into the braze seam. Because Cu and Zr were components of the brazing alloy, it was possible to see that they were distributed evenly throughout the brazing seam in Figure 3e,f. Zone III was primarily concentrated with Ni, Cr, and Co, as seen in Figure 3g,h,i.

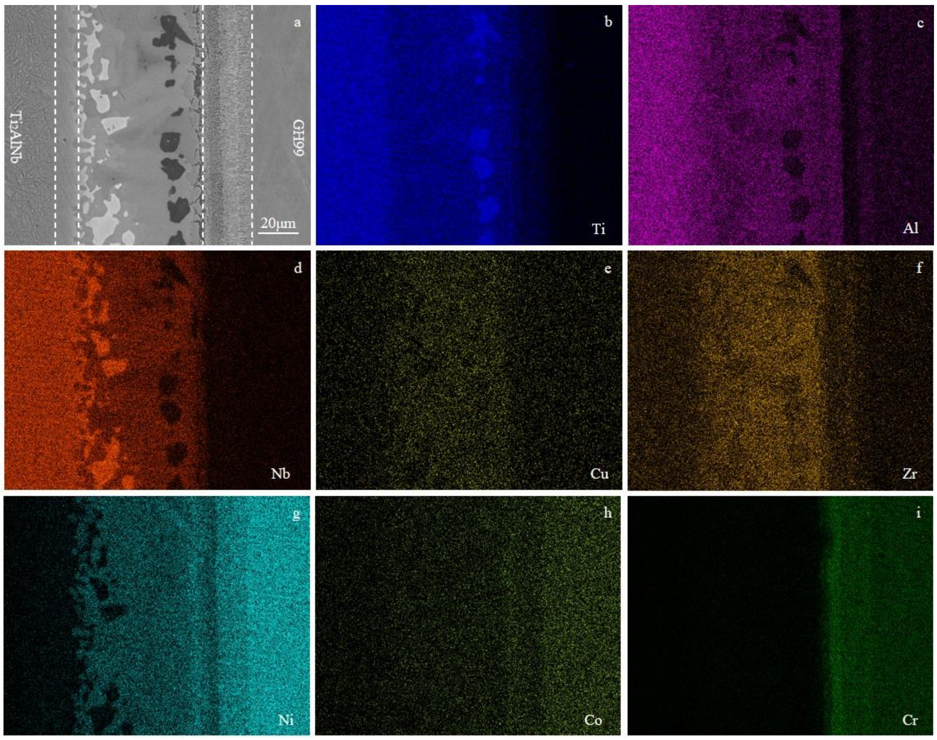

Figure 3. Element distribution maps of the Ti_2AlNb/GH99 joint brazed at 1000 °C for 8 min.

The typical interfacial microstructure of the brazed joint is illustrated in Figure 4. Table 2 displays the findings of the EDS analysis for each phase. The phases marked as A and C had similar atomic percentages. Phase A had more Al elements and fewer Nb elements than the C phase. The phases A and C contained mainly Ti, Al, and Nb elements and the atomic percentages were similar to the B2 phase of the Ti_2AlNb parent metal. Owing to the high relative content of Nb (β phase stabilizer of titanium alloy), phases A and C could be inferred as β/B2 phases, as demonstrated in Ref. [8]. The phases marked as B and D had similar contents consisting mainly of the elements Al, Nb, Ti, and Ni. It can be seen from Table 2 that the atomic percentages of Ti and Ni are close to 2:1. Compared to the

Ti_2Ni phase, the B and D phases had a higher concentration of Al, Nb. Ren et al. also found that the Ti_2Ni phase contains higher Al and Nb elements, and the research suggested that it was the dissolution of these elements in the brazing seam into the Ti_2Ni phase. Therefore, phases B and D were suggested to be Ti_2Ni (Al, Nb) phases, as demonstrated in Refs. [18,19]. In addition, as observed in Figure 5, diffraction peaks of Ti_2Ni were detected on the fracture surface of the Ti_2AlNb side, further proving the formation of Ti_2Ni (Al, Nb) phases in the joint. It could be seen from the ternary phase diagrams [20,21] of Ti-Zr-Cu and Ti-Zr-Ni that Ti was miscible with Zr and Cu was miscible with Ni. In phase E, the atomic percentages of Ti and Zr elements were 64.77%, while Ni and Cu elements were 30.97%. The atomic percentage was close to 2:1, and phase E was identified as the (Ti, Zr)$_2$(Ni, Cu) phase [13]. Similarly, phase F could be considered the (Ti, Zr)(Ni, Cu) phase [17]. In zone III, the phases G, H, and I mainly contained Ni, Cr and Ti elements. With approaching the GH99 side, the content of the Ti element gradually decreased. This indicated the diffusion of elements from the brazing seam into the GH99 alloy. Simultaneously, the elements in GH99 alloy diffused into the brazing seam and eventually converged in the diffusion zone (zone III). According to the Ni-Cr-Ti phase diagram [22], it could be determined that the phases G, H, and I were (Cr, Ni, Ti) ss. Phase J mainly contained Ni and Cr elements. Based on the Ni-Cr binary phase diagram [23], phase J could be determined as (Ni, Cr) solid solution [24]. The XRD analysis identified five phases, which were in agreement with the findings of the EDS analysis, as illustrated in Figure 5: B2/β, (Ti, Zr)(Ni, Cu), (Ti, Zr)$_2$(Ni, Cu), (Ni, Cr) ss, and Ti_2Ni. In conclusion, the microstructure of the interface of the Ti_2AlNb/GH99 joint was Ti_2AlNb alloy/B2/β/Ti_2Ni (Al, Nb) + B2/β + (Ti, Zr)$_2$(Ni, Cu) + (Ti, Zr)(Ni, Cu)/(Cr, Ni, Ti) ss + (Ni, Cr) ss/GH99 superalloy.

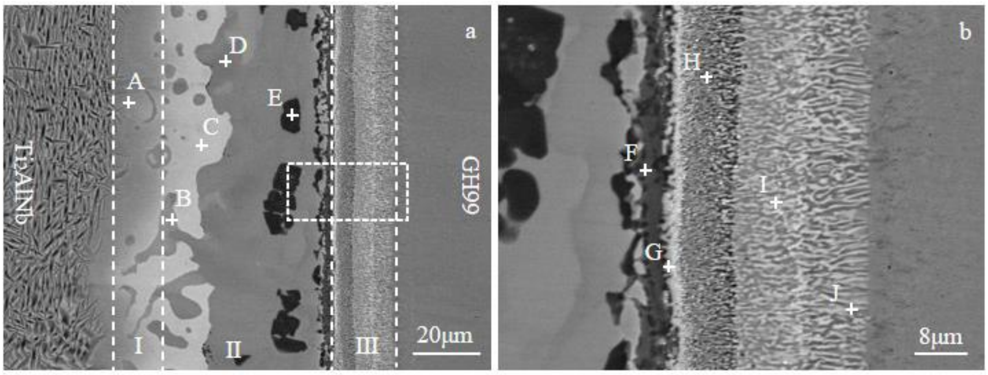

Figure 4. Interfacial microstructure of Ti_2AlNb/GH99 brazed joint (1000 °C/10 min). (**a**) Microstructure of joint interface; (**b**) the GH99 side.

Table 2. EDS analysis of the different phases in Figure 4 (at. %).

Spots	Al	Zr	Nb	Ti	Cr	Co	Ni	Cu	Possible Phase
A	18.33	1.74	22.99	52.50	0.44	0.88	2.37	0.75	β/B2
B	16.08	6.17	11.56	39.57	0.40	1.34	20.41	4.47	Ti_2Ni (Al, Nb)
C	12.56	2.84	29.52	52.80	0.50	0.09	1.33	0.36	β/B2
D	15.07	6.33	10.45	40.53	0.43	1.63	20.92	4.64	Ti_2Ni (Al, Nb)
E	0.24	1.63	1.26	63.14	0.36	2.40	27.95	3.02	(Ti, Zr)$_2$(Ni, Cu)
F	6.41	2.01	1.39	36.40	0.35	4.76	47.45	1.14	(Ti, Zr)(Ni, Cu)
G	5.92	5.36	5.93	19.74	29.76	5.65	27.08	0.56	(Cr, Ni, Ti) ss
H	15.43	2.70	2.03	15.30	28.99	3.90	31.30	0.35	(Ni, Cr) ss
I	2.24	2.08	1.58	14.12	20.26	3.74	55.57	0.41	(Ni, Cr) ss
J	10.26	0.88	1.31	4.74	21.87	5.22	55.45	0.26	(Ni, Cr) ss

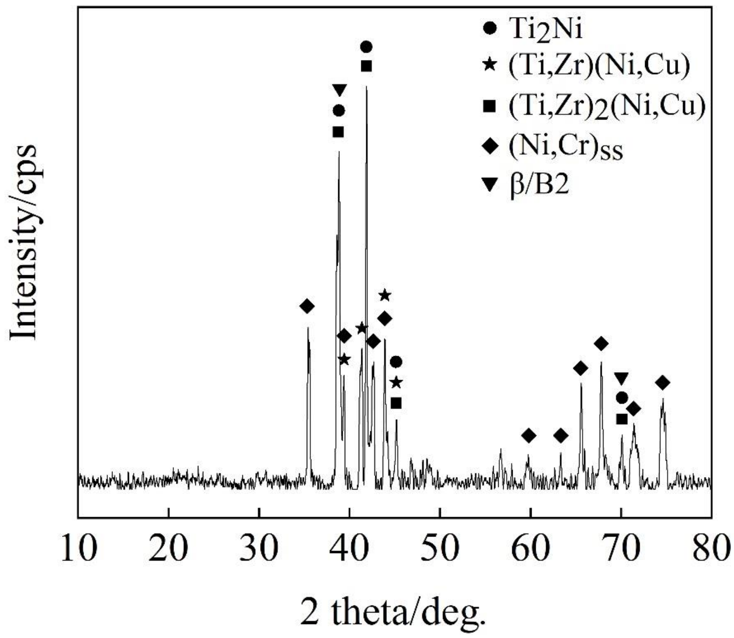

Figure 5. XRD pattern of the fracture surfaces (Ti_2AlNb side) after shear test.

3.2. Effect of Brazing Parameters on the Microstructure of Ti_2AlNb/GH99 Brazed Joints

The BSE diagram of the joint for different brazing temperatures is illustrated in Figure 6. Totally, the brazing temperature had a strong relationship with the interfacial microstructure and the width of brazed joints. Specifically, the widths of zone I and zone II were increased as the brazing temperature rose. The dissolution of the parent metals extended the width of the brazing seam, whereas the melting of the filler alloy had the opposite effect. The brazing alloy used in this experiment was foil, so the effect of the brazing alloy could be ignored. The GH99 dissolved a little, and the increase in braze thickness was mainly due to the melting of Ti_2AlNb. At lower brazing temperatures (960 °C), the Ti_2AlNb/GH99 brazed joints had three distinct reaction zones, as shown in Figure 6a. The reaction zone (zone II) was a distinctly mixed structure. As the brazing temperature increased (1000 °C), the (Ti, Zr)$_2$(Ni, Cu) intermetallic compound decreased, illustrated in Figure 6c. Furter increasing the brazing temperature to 1040 °C, the content of the (Ti, Zr)$_2$(Ni, Cu) phases increased and tended to converge together. However, cracks appeared in the brazing seam (Figure 6e), which would deteriorate the joining properties.

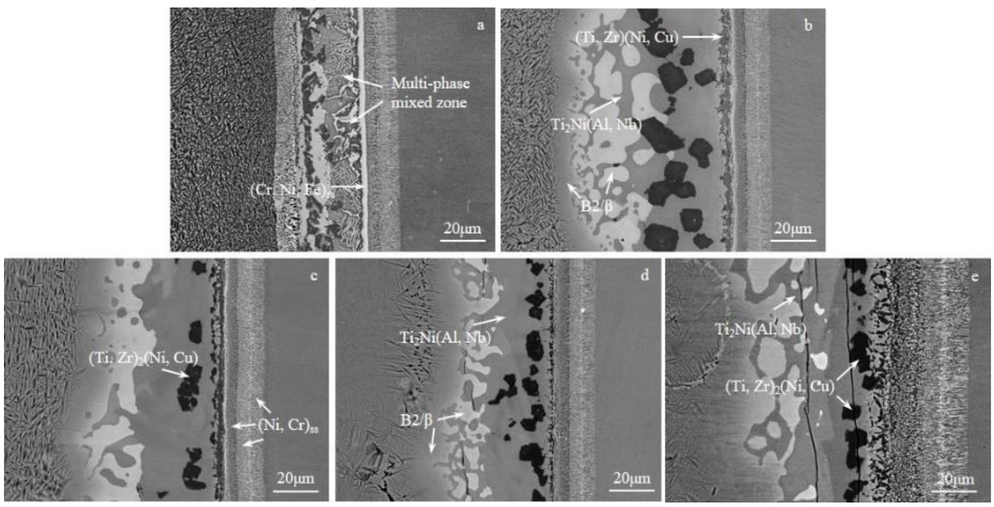

Figure 6. Microstructures of Ti_2AlNb/GH99 joints brazed at different temperatures for 10 min. (**a**) 960 °C; (**b**) 980 °C; (**c**) 1000 °C; (**d**) 1020 °C; (**e**) 1040 °C.

As concluded, the microstructure evolution in brazed joints was influenced by the diffusion and reaction of the filler alloy with the parent metals. Throughout the brazing process, the Ti_2AlNb/GH99 brazed joint interfacial structure changed with temperature in the following way. Firstly, when the brazing temperature was low, the elements such as Al, Nb, Co, and Cr diffused into the brazing seam. Based on the phase diagram of Ti-Cu [24] and Ti-Ni-Al [25], the concentration of Cu and Ni in the liquid pool decreased due to the diffusion and reaction of elements. Meanwhile, the diffusion of elements from Ti_2AlNb alloy to the brazing seam also increased the concentration of Al and Ti in the molten seam, which eventually increased the melting temperature of the liquid phase in the brazing seam. Therefore, an isothermal solidification process occurred even at lower brazing temperatures. It eventually formed lamellar structures near the Ti_2AlNb alloy side. The insufficient reaction between the parent metal and brazing alloy. Continuous (Ti, $Zr)_2$(Ni, Cu) phase and (Ti, Zr)(Ni, Cu) phase distributed in the brazing seam. Compared to the other alloying elements in the GH99 superalloy, Ni had a strong affinity with Ti and was more likely to diffuse into the brazing seam [22]. Thus, other alloying elements in the GH99 were concentrated in zone III, forming the solid solution phase. Secondly, as the brazing temperature increased, more Ti and Ni elements diffused into the Ti_2AlNb side, which promoted the formation of the β/B2 phase and the disappearance of the lamellar structure. Dissolved Al and Nb elements of the Ti_2AlNb alloy aggregated in the brazing seam. The Ti_2Ni (Al, Nb) phase was formed in the brazed seam. Finally, the (Ti, $Zr)_2$(Ni, Cu) and Ti_2Ni (Al, Nb) phase in the brazed seam grew and thickened as the brazing temperature reached 1040 °C. Due to each phase's different thermal expansion coefficients, stress concentration would occur in the cooling process and eventually lead to cracks.

The BSE diagram of the joint for different holding times is illustrated in Figure 7. There was no significant change in interfacial microstructure with increased holding time. The short holding time did not allow the elements in the filler alloy to diffuse sufficiently with the parent metal, and the brazing seam was dominated by the Ti_2Ni (Al, Nb) phase, with less β/B2 phase. With the extension of holding time, the (Ti, $Zr)_2$(Ni, Cu) phase and (Ti, Zr)(Ni, Cu) phase in the brazing seam increased. With extended holding time further, continuous brittle intermetallic compounds were formed in the brazing seam. During the following cooling stage, cracks were generated and propagated along the brittle phase, reducing the strength of brazed joints.

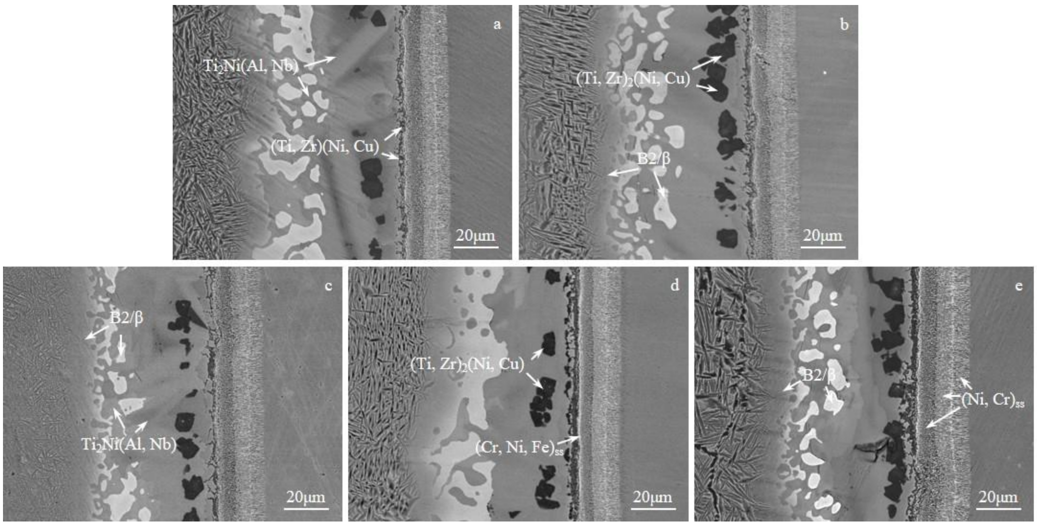

Figure 7. Microstructure of the Ti_2AlNb/GH99 joints brazed at various holding time (1000 °C). (**a**) 4 min; (**b**) 6 min; (**c**) 8 min; (**d**) 10 min; (**e**) 12 min.

Based on the above discussion, the interfacial microstructure evolution during the brazing process is suggested in Figure 8. As the temperature increased to the filler alloy's melting point (853 °C) during the early stages of brazing (as illustrated in Figure 8a), the brazing filler began to melt. The brazing seam had higher concentrations of the elements Ti, Zr, Ni, and Cu. Due to the concentration gradient, Zr and Cu elements diffused to the parent metal on both sides, and Al, Nb, Cr, and Co elements in the parent metals also diffused into the brazing seam. In comparison to elements Cr and Co, the Ni in GH99 superalloy diffused more readily into zone II [22]. The strong affinity for Ni allowed the Ti and Ni in the filler alloy to diffuse to the GH99 and Ti_2AlNb, respectively. With the increase of Ti and Ni concentrations, β-Ti and (Ti, Zr)$_2$(Ni, Cu) were formed during the cooling process, as shown in Figure 8b. Extending the holding time, the element diffused between the parent metal and filler alloy was more adequate. The elements Nb, Ni, and Cu were clustered on the Ti_2AlNb side of the alloy. The maximum solubility of Cu and Ni in β-Ti (13.5 at. % and 10 at. %) was much higher than that of α-Ti, and Nb was a stable element in β phase. The Ti, Nb, and Cu content at higher brazing temperatures was beneficial to the nucleation and growth of β-Ti. Therefore, a diffusion zone (zone I) dominated by the β/B2 phase was formed on the Ti_2AlNb side. In addition, many elements such as Ti, Ni, Nb, and Al were gathered in the brazing seam. According to the existing research, Ni and Ti elements had good affinities, and the Gibbs free energy of 2Ti + Ni = Ti_2Ni was −78.03 KJ/mol [26], so the continuous Ti_2Ni (Al, Nb) phase was formed in the brazing seam. Due to the long-distance diffusion of elements, many Ti, Ni, Zr, and Cu elements were accumulated on the GH99 alloy side, as shown in Figure 3. Finally, a continuous (Ti, Zr) (Ni, Cu) phase was formed on the GH99 side, which hindered the diffusion of Cr and Co into the brazing seam. Eventually, these elements aggregated on the GH99 side (zone III) to form a Ni-Cr-based solid solution, as shown in Figure 8d.

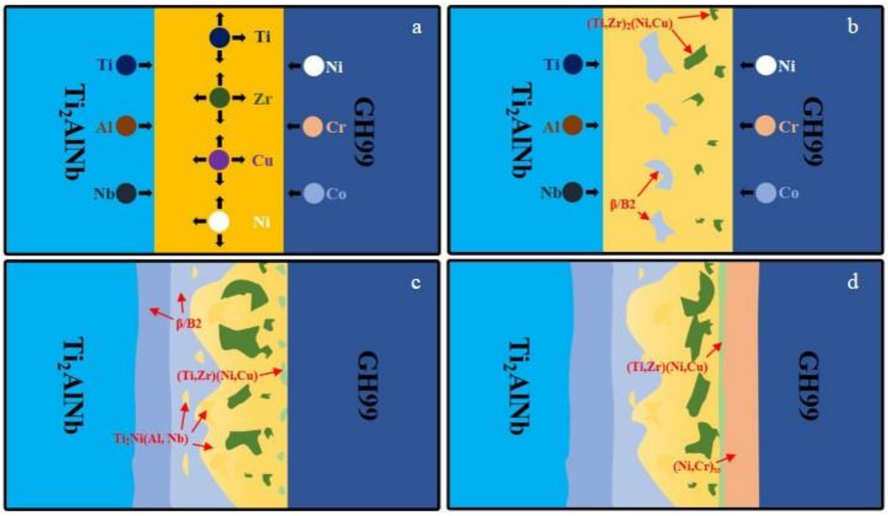

Figure 8. Schematic diagram of the microstructure evolution. (**a**) atomic migration; (**b**) nucleation of β-Ti and (Ti, Zr)$_2$(Ni, Cu); (**c**) nucleation of Ti_2Ni (Al, Nb) and (Ti, Zr)(Ni, Cu); (**d**) final solidification stage.

3.3. Effect of Brazing Parameters on the Mechanical Properties of Ti_2AlNb/GH99 Brazed Joints

The shear strength of the Ti_2AlNb/GH99 brazed joints is shown in Figure 9a,b, respectively, with various processing parameters. With the increase in brazing parameters (temperature or time), the shear strength of the brazed joint increased initially before declining. When the brazing parameters were 1000 °C/8 min, the maximum average shear strength of ~216.2 MPa was achieved. The shear strength was similar to the results of Dong et al. [13]. Further increased brazing parameters resulted in a significant reduction in joint shear strength.

The fracture path of the bonded joint was analyzed by SEM. The fracture paths of the Ti_2AlNb/GH99 brazed joints at various temperatures are shown in Figure 10a–c, and the corresponding fracture surface is shown in Figure 10(a-1–c-1). At different temperatures, the fracture surfaces of the Ti_2AlNb/GH99 joints showed smooth and flat, indicating that the joints were brittle fracture, as shown in Figure 10(a-1–c-1). EDS analysis of the fracture showed that the fracture surface was mainly Ti_2Ni (Al, Nb) phase and (Ti, $Zr)_2$(Ni, Cu) phase when the brazing temperature was below 1000 °C. When the temperature was 1040 °C, the fracture surfaces were Ti_2Ni (Al, Nb), (Ti, $Zr)_2$(Ni, Cu), and (Ti, Zr)(Ni, Cu) phases. Combining Figure 10a–c, it was evident that as the temperature rose, the joint fracture path shifted in favor of the GH99 side. A continuous lamellar organization formed on the Ti_2AlNb side at 960 °C because the reaction between the parent metal and the filler alloy was insufficient at that temperature. These mixed phases became the weak spots in the joint, where most of the fractures occurred. Combined with Figure 9a, it could be seen that the average shear strength of the joint at this temperature was lower at 116.0 MPa. With the increased brazing temperature, the B2/β phase was formed on the Ti_2AlNb side, and the fracture path moved to the brazing seam. Consequently, there was also an increase in joint strength. When the brazing temperature reached 1040 °C, the coarse Ti_2Ni (Al, Nb) and (Ti, $Zr)_2$(Ni, Cu) phases in the brazing seam were also harmful to the joints' properties and caused some microcracks, as illustrated in Figure 10c. It was well known that a continuous metal interlayer was detrimental to the properties of the joint. As a result, the presence of a large number of Ti_2Ni (Al, Nb) layers or continuous (Ti, $Zr)_2$(Ni, Cu) layers of intermetallic compounds in the Ti_2AlNb/GH99 joints obtained at low brazing temperatures (960 °C) or high temperatures (1040 °C) made the brazed joints lower in strength.

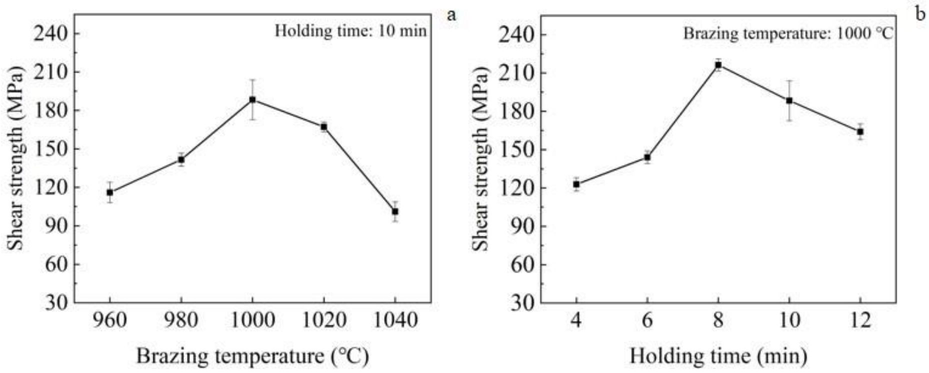

Figure 9. Shear strength of Ti_2AlNb/GH99 joints at various parameters. (**a**) Brazing temperature and (**b**) holding time.

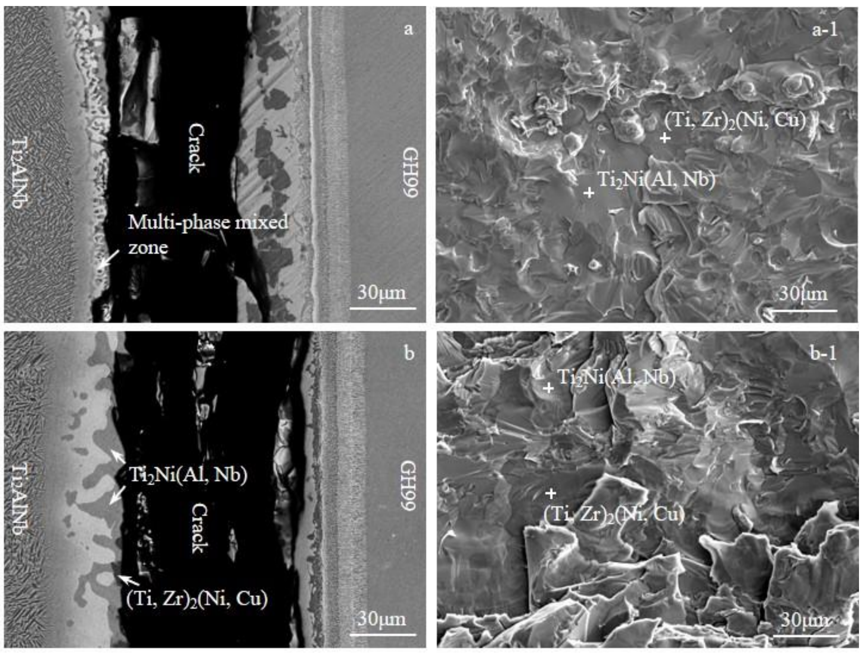

Figure 10. *Cont.*

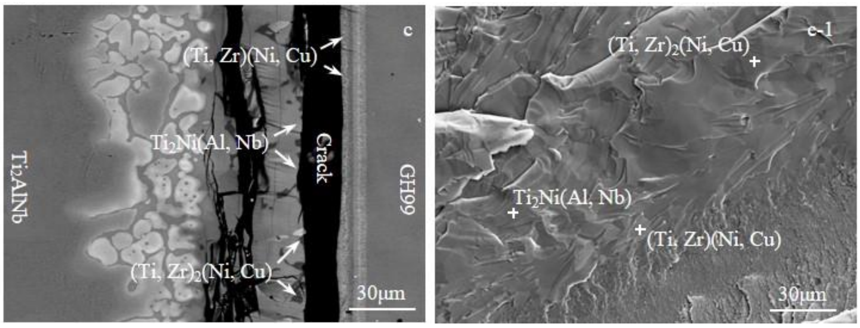

Figure 10. (**a**–**c**) The fracture paths of Ti_2AlNb/GH99 joints at 960 °C, 1000 °C and 1040 °C, respectively (10 min); (**a-1**–**c-1**) the fracture morphology for 960 °C, 1000 °C and 1040 °C, respectively (10 min).

4. Conclusions

Amorphous TiZrCuNi filler was used in this work to successfully braze GH99 superalloy and Ti_2AlNb alloy together. Investigations were carried out into how the interfacial microstructure was affected by the brazing parameters of temperature and time. The interfacial microstructure was related to the mechanical strength of the joint. It provided a theoretical basis for further experimental research. Following was a summary of the key findings:

(1) The characteristic interfacial microstructure of Ti_2AlNb/GH99 joint brazd with TiZrCuNi filler brazed at 1000 °C for 10 min was Ti_2AlNb alloy/B2/β/Ti_2Ni (Al, Nb) + B2/β + (Ti, Zr)$_2$(Ni, Cu) + (Ti, Zr)(Ni, Cu)/(Cr, Ni, Ti) ss + (Ni, Cr) ss/GH99 alloy. The brazing seam was mainly composed of Ti_2Ni (Al, Nb) and (Ti, Zr)$_2$(Ni, Cu) phases.

(2) Higher brazing temperature or longer holding time promoted atomic diffusion between the parent metals and the filler alloy, which enhanced the metallurgical reaction between them, resulting in the increase in Ti_2Ni (Al, Nb) phase and the coarsening of (Ti, Zr)$_2$(Ni, Cu) phase.

(3) The existence of coarse (Ti, Zr)$_2$(Ni, Cu) phase and continuous Ti_2Ni (Al, Nb) phase in the brazing seam resulted in cracks that could easily sprout and expand in these brittle phases, and the performance of Ti_2AlNb/GH99 brazed joint was decreased dramatically. The joints reached a maximum average shear strength of ~216.2 MPa when brazed at 1000 °C for 8 min. The fracture results showed that the cracks extend in the brazed seam.

Author Contributions: Conceptualization, S.H.; methodology, J.C.; software, J.C.; validation, S.H. and H.L.; investigation, J.C.; resources, S.H. and H.L.; date curation, J.C.; writing—original draft preparation, J.C.; writing—review and editing, S.H. and J.C.; visualization, S.H.; supervision, D.L. and W.F.; project administration, S.H.; funding acquisition, X.S. All authors have read and agreed to the published version of the manuscript.

Funding: The authors gratefully acknowledge the financial support from the National Natural Science Foundation of China (Grant Nos. 51905125, 52175307 and 52105330) and the Taishan Scholars Foundation of Shandong Province (No. tsqn201812128).

Data Availability Statement: The date that support the findings of this study are available within the article.

Conflicts of Interest: The authors declare no conflict of interest.

References

1. Pollock, T.M.; Tin, S. Nickel-based superalloys for advanced turbine engines: Chemistry, microstructure, and properties. *J. Propul. Power* **2006**, *22*, 361–374. [CrossRef]
2. Wang, P.; Chen, D.; Fan, J.; Sun, K.; Wu, S.; Li, J.H.; Sun, Y. Study on the influence of process parameters on high performance Ti-6Al-4V parts in laser powder bed fusion. *Rapid Prototyp. J.* 2022; *ahead-of-print*. [CrossRef]

3. Wang, Y.; Shao, W.Z.; Zhen, L.; Yang, L.; Zhang, X.M. Flow behavior and microstructures of superalloy 718 during high temperature deformation. *Mater. Sci. Eng. A-Struct. Mater. Prop. Microstruct. Process.* **2008**, *497*, 479–486. [CrossRef]
4. Nespoli, A.; Bennato, N.; Villa, E.; Passaretti, F. Study of anisotropy through microscopy, internal friction and electrical resistivity measurements of Ti-6Al-4V samples fabricated by selective laser melting. *Rapid Prototyp. J.* **2022**, *28*, 1060–1075. [CrossRef]
5. Farzaneh, A.; Khorasani, M.; Farabi, E.; Gibson, I.; Leary, M.; Ghasemi, A.M.H.; Rolfe, B.F. Sandwich structure printing of Ti-Ni-Ti by directed energy deposition. *Virtual Phys. Prototyp.* **2022**, *17*, 1006–1030. [CrossRef]
6. Chen, R.R.; Dong, S.L.; Guo, J.J.; Ding, H.S.; Su, Y.Q.; Fu, H.Z. Microstructure evolution and mechanical properties of directionally-solidified TiAlNb alloy in different temperature gradients. *J. Alloys Compd.* **2015**, *648*, 667–675. [CrossRef]
7. Kesler, M.S.; Goyel, S.; Ebrahimi, F.; Manuel, M.V. Effect of microstructural parameters on the mechanical behavior of TiAlNb(Cr,Mo) alloys with gamma plus sigma microstructure at ambient temperature. *J. Alloys Compd.* **2017**, *695*, 2672–2681. [CrossRef]
8. Cai, X.Q.; Wang, Y.; Yang, Z.W.; Wang, D.P.; Liu, Y.C. Transient liquid phase (TLP) bonding of Ti2AlNb alloy using Ti/Ni interlayer: Microstructure characterization and mechanical properties. *J. Alloys Compd.* **2016**, *679*, 9–17. [CrossRef]
9. Prasad, K.S.; Rao, C.S.; Rao, D.N. Effect of process parameters of pulsed current micro plasma arc welding on weld pool geometry of Inconel 625 welds. *Met. Mater.* **2012**, *50*, 175–181. [CrossRef]
10. Cai, X.L.; Sun, D.Q.; Li, H.M.; Meng, C.; Wang, L.; Shen, C.J. Dissimilar joining of TiAl alloy and Ni-based superalloy by laser welding technology using V/Cu composite interlayer. *Opt. Laser Technol.* **2019**, *111*, 205–213. [CrossRef]
11. Gaikwad, V.T.; Mishra, M.K.; Hiwarkar, V.D.; Singh, R.K.P. Microstructure and mechanical properties of friction welded carbon steel (EN24) and nickel-based superalloy (IN718). *Int. J. Miner. Metall. Mater.* **2021**, *28*, 111–119. [CrossRef]
12. Ren, X.; Ren, H.; Shang, Y.; Xiong, H.; Zhang, K.; Zheng, J.; Liu, D.; Lin, J.; Jiang, J. Microstructure evolution and mechanical properties of Ti2AlNb/TiAl brazed joint using newly-developed Ti–Ni–Nb–Zr filler alloy. *Prog. Nat. Sci. Mater. Int.* **2020**, *30*, 410–416. [CrossRef]
13. Dong, D.; Shi, K.; Zhu, D.; Liang, Y.; Wang, X.; Wei, Z.; Lin, J. Microstructure evolution and mechanical properties of high Nb–TiAl alloy/GH4169 joints brazed using CuTiZrNi amorphous filler alloy. *Intermetallics* **2021**, *139*, 107351. [CrossRef]
14. Sequeiros, E.W.; Guedes, A.; Pinto, A.M.P.; Vieira, M.F.; Viana, F. Microstructure and Strength of gamma-TiAl alloy/Inconel 718 brazed joints. In Proceedings of the 6th International Materials Symposium (MATERIALS 2011)/15th Meeting of SPM, Guimaraes, Portugal, 18–20 April 2011; pp. 835–840.
15. Ren, H.S.; Xiong, H.P.; Long, W.M.; Chen, B.; Shen, Y.X.; Pang, S.J. Microstructures and mechanical properties of Ti3Al/Ni-based superalloy joints brazed with AuNi filler metal. *J. Mater. Sci. Technol.* **2019**, *35*, 2070–2078. [CrossRef]
16. Liu, D.; Song, Y.; Shi, B.; Zhang, Q.; Song, X.; Niu, H.; Feng, J. Vacuum brazing of GH99 superalloy using graphene reinforced BNi-2 composite filler. *J. Mater. Sci. Technol.* **2018**, *34*, 1843–1850. [CrossRef]
17. Li, X.; Li, L.; Hu, K.; Qu, S. Vacuum brazing of TiAl-based intermetallics with Ti–Zr–Cu–Ni–Co amorphous alloy as filler metal. *Intermetallics* **2015**, *57*, 7–16. [CrossRef]
18. Wang, G.; Wu, P.; Wang, W.; Zhu, D.D.; Tan, C.Q.; Su, Y.S.; Shi, X.Y.; Cao, W. Brazing Ti-48Al-2Nb-2Cr Alloys with Cu-Based Amorphous Alloy Filler. *Appl. Sci.* **2018**, *8*, 920. [CrossRef]
19. Ren, H.; Ren, X.; Long, W.; Chen, B.; Pang, S.; Xiong, H. Formation mechanism of interfacial microstructures and mechanical properties of Ti2AlNb/Ni-based superalloy joints brazed with NiCrFeSiB filler metal. *Prog. Nat. Sci. Mater. Int.* **2021**, *31*, 310–318. [CrossRef]
20. Raghavan, V. Handbook of ternary alloy phase diagrams. *J. Phase Equilib. Diffus.* **2006**, *27*, 371. [CrossRef]
21. Lee, M.K.; Kim, K.H.; Lee, J.G.; Rhee, C.K. Growth of isothermally-solidified titanium joints using a multi-component Zr-Ti-Cu-Ni-Be amorphous alloy as a brazing filler. *Mater. Charact.* **2013**, *80*, 98–104. [CrossRef]
22. Li, H.; Wei, H.; He, P.; Lin, T.; Feng, J.; Huang, Y. Effects of alloying elements in GH99 superalloy on microstructure evolution of reactive brazing TiAl/GH99 joints. *Intermetallics* **2013**, *34*, 69–74. [CrossRef]
23. He, P.; Wang, J.; Lin, T.; Li, H. Effect of hydrogen on diffusion bonding of TiAl-based intermetallics and Ni-based superalloy using hydrogenated Ti6Al4V interlayer. *Int. J. Hydrogen Energy* **2014**, *39*, 1882–1887. [CrossRef]
24. Hayama, A.O.F.; Andrade, P.N.; Cremasco, A.; Contieri, R.J.; Afonso, C.R.M.; Caram, R. Effects of composition and heat treatment on the mechanical behavior of Ti–Cu alloys. *Mater. Des.* **2014**, *55*, 1006–1013. [CrossRef]
25. Schuster, J.C.; Pan, Z.; Liu, S.; Weitzer, F.; Du, Y. On the constitution of the ternary system Al–Ni–Ti. *Intermetallics* **2007**, *15*, 1257–1267. [CrossRef]
26. Zhang, B.C.; Chen, J.; Coddet, C. Microstructure and Transformation Behavior of in-situ Shape Memory Alloys by Selective Laser Melting Ti-Ni Mixed Powder. *J. Mater. Sci. Technol.* **2013**, *29*, 863–867. [CrossRef]